AUTHORS' POSTPRINT Originally published in AIP Conference Proceedings 1999, 040009 (2018); https://doi.org/10.1063/1.5049272

Novel Mask-less Plating Metallization Route for Bifacial Silicon Heterojunction Solar Cells

Thibaud Hatt[1, a)], Vivek P. Mehta[1, b)], Jonas Bartsch[1, c)], Sven Kluska[1, d)], Mike Jahn[1, e)], Dietmar Borchert[2, f)], Markus Glatthaar[1, g)]

[1]*Fraunhofer Institute for Solar Energy Systems ISE, Heidenhofstraße 2, 79110 Freiburg, Germany*
[2]*Fraunhofer Institute for Solar Energy Systems ISE, Auf der Reihe 2, 45884 Gelsenkirchen, Germany*

[a)]Corresponding author: thibaud.hatt@ise.fraunhofer.de
[b)]vivek.pankaj.mehta@ise.fraunhofer.de
[c)]jonas.bartsch@ise.fraunhofer.de
[d)]sven.kluska@ise.fraunhofer.de
[e)]mike.jahn@ise.fraunhofer.de
[f)]dietmar.borchert@ise.fraunhofer.de
[g)]markus.glatthaar@ise.fraunhofer.de

Abstract. The proof of concept of a novel metallization route for bifacial silicon heterojunction (SHJ) solar cells by selective plating – i.e. organic mask-free, is demonstrated by a first lab scale solar cell (η=15.5%). A patterned metal-seed is inkjet-printed or deposited by PVD on a PVD-Al layer covering the ITO layer. The copper electroplating process is investigated considering different electrolytes and plating settings in order to selectively cover the metal-seed and not the PVD Al layer. As well a processing chemistry to etch the PVD-Al layer without affecting the ITO and the electroplated contact is presented.

INTRODUCTION

The metallization of the contacts for SHJ solar cells is currently of high interest and several routes through electroplating are studied [1–10]. Plating of copper on transparent conductive oxides (TCOs) becomes more interesting due to the unpredictable fluctuations of the silver price in the market and the low conductivity of screen-printed contacts on SHJ solar cells [11–12]. The low temperatures required for the plating process, the high conductivity of the contacts and patterning of the bifacial metal grid at the same time makes low-cost electroplated contacts a very interesting metallization.

The TCO surfaces of the SHJ solar cells have to be masked or modified to design the contact grid and to avoid the metal electrodeposition on the conductive TCOs. The field of microelectronics already supplied a metallization approach for copper bifacial plating of large area SHJ solar cells with the perspective for implementation at an industrial scale. This "State of the Art" – i.e. reference plating process, applied by research institutes and some industrial players consists of using a patterned organic negative mask to define the metal grid [7-10]. Below the organic mask – i.e. on the TCO, a metal layer deposited by physical vapour deposition (PVD) acts as fast and homogeneous electroplating promoter. After contact metallization, the organic negative mask is stripped and the PVD metal layer is etched in non-grid positions. This metallization route already obtained high efficiencies of up to 24% on bifacial six inch SHJ solar cells [10]. Further improvement of the plating metallization with even more cost-effective process might challenge the well-known screen-printing technology.

Our novel route described by the process sketch in Figure 1 consists of depositing a patterned metal-seed on a self-passivated aluminum layer acting as current distribution promoter. Furthermore, the self-passivated surface of the aluminum provides a better inhibition than TCOs to plate selectively the contacts of the SHJ solar cell [13–14]. Similar

to the reference plating process, a thin metal layer is deposited on both sides of the cell by PVD after TCO deposition. Since this can be achieved within the same processing tool, without breaking the vacuum, this step does not contribute importantly to the manufacturing costs. In contrast to the reference plating process (using organic mask stripped after contact plating), a metal-seed is either deposited by PVD or printed to define the positive grid (other options are available [6, 14]). In the next step, a copper layer is electroplated selectively onto the metal-seed, leaving the self-passivating aluminum layer free of copper. A few nanometers of silver are used to cap the copper contacts to prevent copper oxidation and therefore increasing the solar cell durability. As can be seen in the drawing, our Ag-capping covers the entire Cu contact without leaving bare Cu surface as it is the case in the reference plating process. In the last step, we remove selectively the PVD metal deposited on the TCO by chemical processing. The described process additionally allows for a simultaneous bifacial metallization of the SHJ solar cells. A promising SHJ solar cell was plated by our mask-less plating metallization and thereby demonstrates a proof-of-concept.

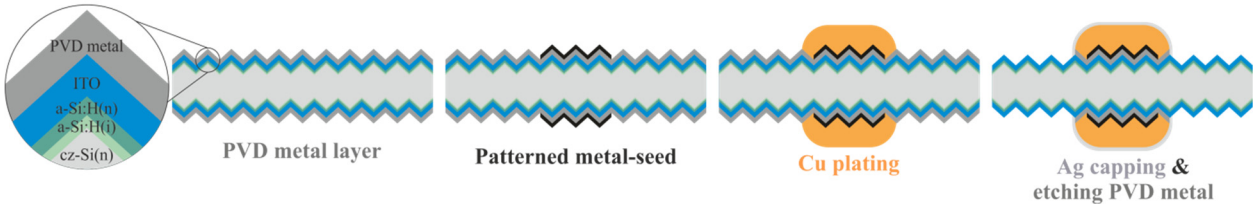

FIGURE 1. Sketch of the novel mask-less metallization route by plating for bifacial SHJ solar cells.

EXPERIMENTAL DETAILS

Our investigations on selective copper plating, PVD metal etching and metallization processing of SHJ solar cell were performed on two different precursor types. The selective electrodeposition of copper was carried out on n-type Cz-Si wafers from *NorSun* (1-3 Ω.m) taken after texturing and dicing (5cm x 5cm). A metal stack composed of 30 nm of Ni covered by 100 nm of Al was deposited by PVD on one side of the textured Si surface. A patterned metal-seed (1 Busbar and 19 Fingers) formed by 5 nm of Cr and 500 nm of Ag was then e-gun deposited through a mask onto the self-passivated aluminum layer. The electrolyte influence on the copper plating selectivity was first studied. Four aqueous copper sulphate or pyrophosphate-based electrolytes were prepared and stirred in beakers. These commercial and self-made electrolytes present different compositions and pH values (<1.0 to 8.4). A forward/reverse pulsed current was used to plate selectively on the Cr/Ag metal-seed. This pulse plating process increases the selectivity by favoring plating on large Cu seeds while parasitic seeds are dissolved during reverse current due to their larger surface/volume ratio. The electrical contact of the sample to plate copper is realized by a clamp on the edge. A medium current density of 6 A/dm², forward and reverse current pulse times of 15 ms and 1 ms respectively and a high anodic to cathodic current ratio of 4.5 were applied. The samples were then cleaned in DI water and dried with air. The selectivity of the plating process of each sample was assessed by optical inspection and the copper morphology was characterized with a Schottky emission scanning electron microscope (SEM) SU-70 from *Hitachi*.

The experiments to optimize the plating settings were carried out in the copper sulphate-based electrolyte with lowest acidity (pH 3.3). Direct-current (DC) or pulse plating with a medium current density of 6 A/dm² was applied. For the pulse plating, a variation of the anodic to cathodic ratio (1.5 ; 3 ; 4.5) was studied without modifying the pulse times described above. The current density was then increased from 6 to 12 and 20 A/dm² to reduce the plating time to a few minutes. A macroscopic observation of the selective copper deposition allows detecting parasitic plating.

The etching and the metallization of SHJ solar cells were carried out on industrial standard 156 x 156 mm² n-type Cz SHJ precursors, taken out of the process after indium tin oxide (ITO) sputtering – i.e. before contacts metallization. These bifacial precursors present a textured silicon surface covered by a thin intrinsic amorphous hydrogenated silicon layer – i.e. a-Si:H(i) followed by a doped a-Si:H(n / p-type) passivating layer. The a-Si:H (n / p-type) layers are covered by ITO as shown in Figure 1. The front side of the precursors was either covered by 100 nm of Ag, Cu or Al deposited by PVD. The cells were diced into smaller pieces for lab accommodation. Strong aqueous acid etchants composed of HCl, HNO_3 or a blending of H_3PO_4 – HNO_3 – CH_3COOH were prepared. Alkaline aqueous NH_3 or NH_4OH based solutions were also prepared and blended with H_2O_2 as described in Table 1. The PVD metals were then dipped into the different mixtures for a few seconds or minutes until complete removal of the metal layers. The phosphoric acid-based etchant was set to a temperature of 50°C. A bath of DI water was used to clean the samples directly after etching. The etching times were determined by macroscopic and microscopic observations.

The industrial SHJ precursors were also used to determine the ITO stability against our selected etchants. Before chemical processing, the sheet-resistance R_{sh} of the ITO layer was measured by the Four-point probe method detailed by Smits [15]. The R_{sh} of the ITO layer was then again measured after the metal etching process. For a SEM analysis of the ITO thickness prior and after the processing, cross sections were prepared by cleaving.

Another batch of SHJ precursors was processed by our metallization process to produce actual solar cells. A metal stack composed of 20 nm of Ag and 100 nm of Al was sputtered on both sides of the precursors after a short plasma treatment. The thin layer of Ag acts as a diffusion barrier, preventing the diffusion of Al into the ITO. The Al metal layer was then covered by a patterned metal-seed, inkjet-printed with a PIXDRO LP50 printer from Meyer Burger. The particle-free reactive silver ink [16] was synthetized in our lab and then printed in fine lines (down to 20 µm) to form the patterned metal-seed. During the printing process, the ink reacts and forms fine Ag particles on top of the Al layer. The optimal pulse plating settings determined above allowed the selective copper plating onto the Ag-seed lines without parasitic plating. A thin Ag capping was plated by DC plating in a commercial alkaline electrolyte. After contact metallization, the PVD metals (Al and Ag) were both etched unexpectedly by the phosphoric-nitric acid mixture. The metallized SHJ solar cell was subsequently cleaned in DI water and dried by air before characterization by SEM. The contact resistivity was measured by using the transfer length method (TLM) [17]. The 1-sun current voltage (I-V) parameters of the solar cell were measured under standard testing conditions (STC: AM1.5g, 100 mW/cm²) using a sun-simulator.

RESULTS AND DISCUSSIONS

Selective Electrodeposition of Copper

Better selective copper plating on only the PVD Cr/Ag-seed and not on the entire PVD Al was reached for two of the four tested electrolytes. It should be noted that 1 to 3 nm of aluminum oxide – i.e. alumina Al_2O_3 [18], are growing on the PVD Al layer surface when exposed to oxygen. This thin oxide surface is sufficient to plate Cu selectively on the nobler Ag-seed as demonstrated in the following. The electrolytes' pH, among other properties like chemical composition, has an obvious influence on the selectivity of the copper plating as observed in Figure 2 (a). The acidic, sulphate-based copper electrolytes (pH below 1 and 2.8) lead to parasitic copper plating on the Al layer. The phenomenon is much more pronounced for lower pH values and is mainly due to the chemical instability of the Al_2O_3 present at the Al surface. Indeed, in accordance with the Pourbaix diagram of aluminum [19], low pH causes instability – in this case dissolution of the ultra-thin Al_2O_3 passivation layer. Significant stability differences of the alumina are observed for pH values between 2 and 4, depending on the dissolved concentrations. The Al_2O_3 is only stable for pH values above 4 and the thermodynamic driving force for the oxide dissolution increases for decreasing pH. For low acidity (pH 3.3), no parasitic plating is observed, synonym of excellent Cu plating selectivity. The slight alkalinity of the pyrophosphate-based electrolyte is on the other hand at the limit of the alumina stability and could thereby explain the high density of parasitic plating observed on the plated sample. Such an alkaline electrolyte, held at a pH below 8.0, would give a better selectivity according to the Pourbaix diagram. Investigations on how to reduce the pH of such an electrolyte are ongoing.

The structural morphology of the plated Cu is significantly affected by the electrolyte characteristics. The SEM pictures shown in Figure 2 (b) allow observing the growth pattern of the dense and compact Cu plated on the Ag-seed. In the two electrolytes which lead to high parasitic plating, the amount of Cu deposited on the Ag seed is quite low. Still, it can be observed that the structure of the Cu deposited on the Ag-seed and the parasitic Cu on the Al layer differs. The parasitic Cu presents few seeds that are not linked. This characteristic growth may be due to a locally higher oxide concentration on the Al surface. On the other hand, the Cu structure on the Ag-seed is compact and uniform. Because of the large amount of parasitic Cu, only a thin layer of Cu is plated onto the Ag-seed. This is why in this case the pyramid structure of the underlying silicon is still visible. At least, the Cu structure seems to be smoother in the Cu_2PO_7. The sample with less parasitic plating (pH 2.8) presents a sharp nodular growth of the Cu. It should be noted that this commercial electrolyte is designed for DC electroplating. Enough Cu was deposited on the Ag-seed to hide the Si pyramids surface. The parasitic Cu plating is mainly located close to the Ag-seed due to the higher electron concentration in these regions. The best electrolyte, leading to no parasitic copper, shows a nice compact structure. This dense morphology is required to reach high conductivity and therefore allows a reduction of the plated contact height and width – i.e. lowering the plating time and metal consumption for solar cells.

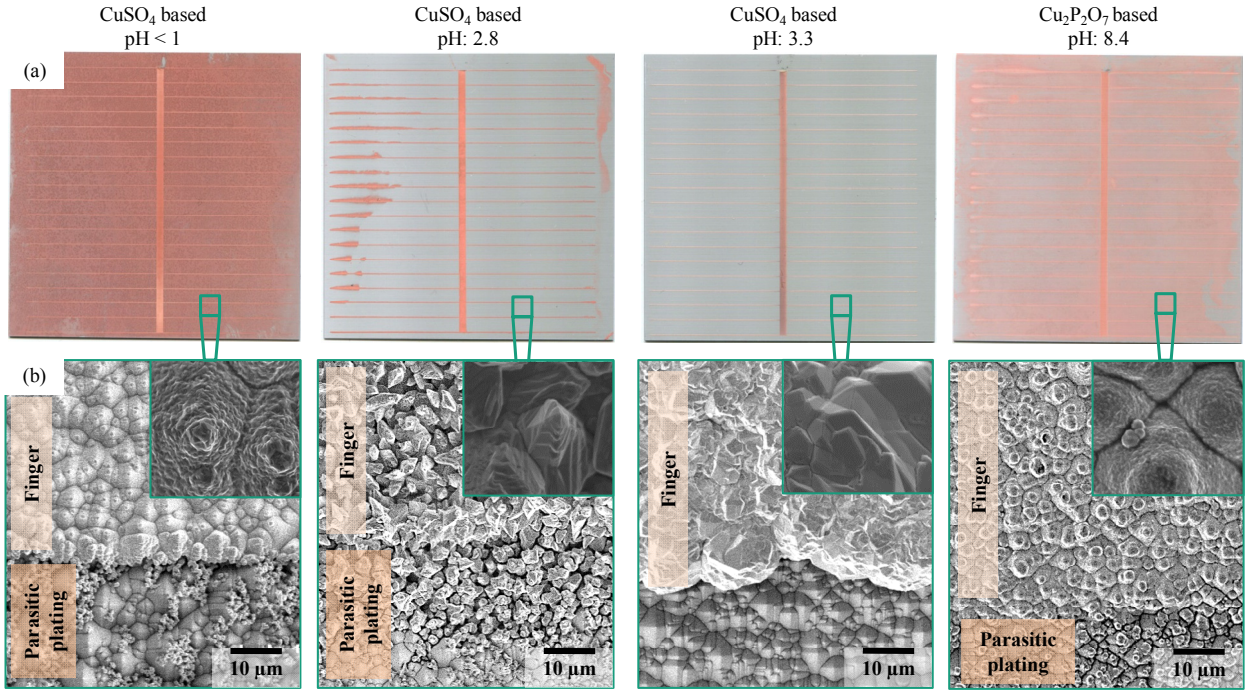

FIGURE 2. (a) Samples covered by PVD Al and a grid of Cr/Ag plated with Cu in different electrolytes, (b) SEM top view of the above fingers plated with copper.

Plating settings to get 100% of the Cu deposition on the Cr/Ag-seed were reached in the low acidity $CuSO_4$-based electrolyte (pH 3.3). As observed in Figure 3, DC plating leads to significant parasitic plating at the rim of the sample where higher field density can be expected. Pulse plating with a small anodic/cathodic current ratio (R=1.5) shows already a much better plating selectivity. This forward/reverse pulsed current allows strengthening the nucleation on conductive sites. Parasitic Cu, which might be deposited on the Al_2O_3 surface due to electron tunneling, is quickly removed during Cu oxidation. An increase in current ratio to 4.5 at the same current density avoids parasitic plating. Samples plated with these settings show excellent selectivity of the Cu deposition. Increasing the current density to 12 A/dm² to plate the samples faster affects the selectivity. This phenomenon could be explained by the higher electron concentration, which increases the probability of parasitic Cu deposition. As expected, 20 A/dm² lead to even more parasitic plating and wider Cu fingers. Nevertheless, the plating time is already in an applicable range for industrial electroplating (6 A/dm², 6 min for 5 µm of Cu).

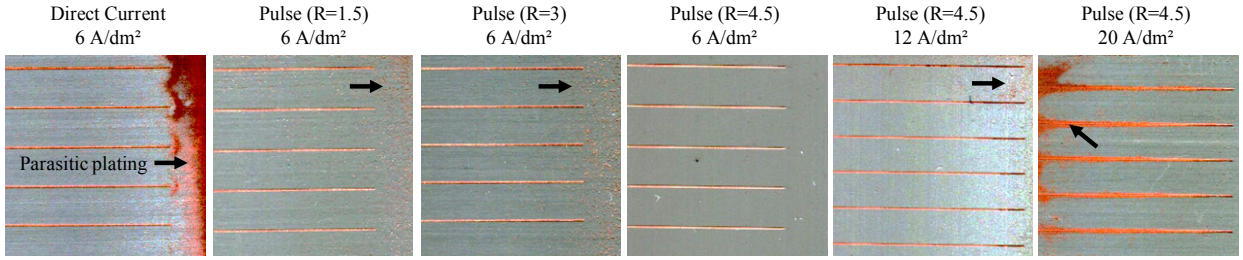

FIGURE 3. Enlarged views of the selective copper plated in the $CuSO_4$-based electrolyte (pH 3.3) in dependence on DC and pulse plating, different anodic to cathodic current ratio and current densities.

Etching of PVD Metal Stack

Each PVD metal deposited on the ITO from SHJ precursors needs a specific etching solution. The strong acids (hydrochloric or nitric acids, 10% and 15% respectively) lead to a fast lift-off of the full Ag layer as a foil. The metallic bonds between Ag atoms seem to be intact meaning that the adhesion loss could be explained by a modification of the hydroxyl groups at the ITO / Ag interface. Preventing this effect is important to avoid the lift-off of the plated contacts from the ITO of SHJ solar cells. In contrast, alkaline and medium acidic solutions as described in Table 1 were suitable to etch the different metals. Silver is faster etched than copper in the ammonia-based solution and the opposite is observed in the phosphoric acid-based etchant. The different metal etching rates are due to the chemical reaction and Gibbs free energy of oxidation. Further studies are ongoing to determine the metal etching rates for our specific application. The Al layer, presenting a native oxide surface, does not seem affected by these alkaline solutions while showing a fast etching rate in the phosphoric-based acidic solution. A strong under-etching below the contacts was observed with this etchant. The under-etching was reduced by increasing the etchant temperature and thereby reducing the processing time.

TABLE 1. Table of etchants of PVD metal layers and sheet resistance of the ITO of SHJ solar cell measured by 4-Point probe method on the sample after etching.

Etchant	**Etching time of PVD metal**			**R_{sh} ITO**	
	Ag	Cu	Al_2O_3 - Al	Front	Rear
(Volume ratio)	*(s)*	*(s)*	*(s)*	*(Ω/sq)*	*(Ω/sq)*
$NH_4OH – H_2O_2 – H_2O$ (2:1:10) @ 25°C	15	60	> 600	~ 125	~ 185
$NH_3 – H_2O_2 – H_2O$ (1:1:9) @ 25°C	15	120	> 600	-	-
$H_3PO_4 – HNO_3 – CH_3COOH – H_2O$ (80:5:5:10) @ 50°C	2	1	5	~ 130	~ 190

The sheet resistance R_{sh} of the ITO covering the SHJ precursors was measured to be around 130 Ω/sq and 190 Ω/sq respectively for the front and rear sides. The higher ITO R_{sh} measured on the rear side is due to a different ITO doping and the a-Si:H(p) layer underneath. After dipping for a few minutes in the etchants, the ITO R_{sh} does not change significantly as noticed in Table 1. Nevertheless, a longer dipping in the acidic solution affects significantly the ITO on the rear side contrary to the alkaline solution. The R_{sh} changes confirm the use of the Four-point probe method to characterize a modification of the ITO layer.

A deeper investigation by SEM confirms the results above – i.e. the ITO stability as shown in Figure 4. The thickness of the ITO layers was measured around 70 ± 5 nm for the reference and the dipped samples. The surface morphology of the ITO presenting a fine grained structure remains the same too. These investigations confirm these etchants for the removal of the PVD metals at the end of our novel metallization process without damaging the ITO layer.

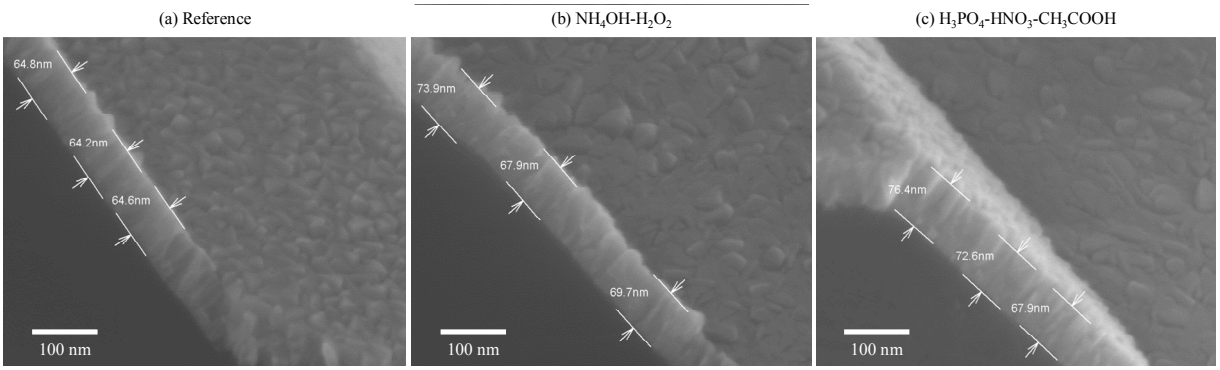

FIGURE 4. Scanning electron microscopy images on cross-section of the front side of SHJ solar cells covered by a thin ITO layer, (a) reference before contact with etchant, after dipping in aqueous solution of (b) $NH_4OH – H_2O_2$ and (c) $H_3PO_4 – HNO_3 – CH_3COOH$.

Solar Cells Properties

Promising first efficiencies were reached for several lab scale SHJ solar cells metallized by our novel plating route. For lab accommodation we processed small monofacial solar cells diced from a 6 inch precursor. The plated fingers of the cell are compact and show a good adhesion on the SHJ precursor. The cell is almost free of parasitic plating. The electrical performance is still limited by several factors, such as the small area to rim ratio (diced rim inducing recombination losses as already studied by Rauer *et al*. [20]), non-optimized inkjetting procedure and non-optimized rear side metallization for the monofacial architecture. This is why the first cell efficiency obtained only 15.5%. The contact resistivity measured on this cell was found to be at 1 $m\Omega \cdot cm^2$, which is an extremely encouraging result already at this early development stage.

CONCLUSION & OUTLOOK

Processing routes featuring selective plating on a PVD or printed metal seed on self-passivated PVD metal layers are interesting to challenge the screen-printing metallization technology. Furthermore, this shorter process avoids the organic mask stripping step of the reference plating process. Continuous metal-seed grids were either PVD deposited or inkjet-printed with a particle free reactive silver ink. A $CuSO_4$-based electrolyte was found to obtain highly selective copper plating onto these metal-seeds on PVD Al surfaces. The pulse plating settings were optimized to fully erase parasitic plating. Several etchants demonstrate to be suitable to etch the PVD metal layer without damaging the thin ITO layer on the solar cell. A first promising efficiency of 15.5% and a contact resistivity of 1 $m\Omega \cdot cm^2$ were reached with our novel mask-less metallization process through plating. Further optimization is ongoing to fully exploit the efficiency potential of SHJ solar cells with this new approach in the near future.

ACKNOWLEDGMENTS

The colleagues at ISE are acknowledged for fruitful discussion and technical assistance. The authors especially would like to thank P. Schäfer, S. Bogatti, J. Eckert, R. Haberstroh, F. Martin, E. Schäffer and M. Wichmann for sample preparation and measuring the solar cells. This work was funded by the European project DISC under the European Union's Horizon 2020 research and innovation program under grant agreement N°727529.

REFERENCES

1. S. de Wolf, A. Descoeudres, Z. C. Holman, and C. Ballif, green 2 (2012).
2. D. Erath, M. Pospischil, R. Keding, M. Jahn, I. Lacmago Lontchi, A. Lorenz, and F. Clement, Energy Procedia 124, 869 (2017).
3. A. Khanna, K.-U. Ritzau, M. Kamp, A. Filipovic, C. Schmiga, M. Glatthaar, A. G. Aberle, and T. Mueller, Applied Surface Science 349, 880 (2015).
4. K. Yoshikawa, H. Kawasaki, W. Yoshida, T. Irie, K. Konishi, K. Nakano, T. Uto, D. Adachi, M. Kanematsu, H. Uzu, and K. Yamamoto, Nat. Energy **2**, 17032 (2017).
5. D. Adachi, T. Terashita, T. Uto, J. L. Hernández, and K. Yamamoto, Solar Energy Materials and Solar Cells 163, 204 (2017).
6. A. Rodofili, W. Wolke, L. Kroely, M. Bivour, G. Cimiotti, J. Bartsch, M. Glatthaar, and J. Nekarda, Sol. RRL 1, 1700085 (2017).
7. A. Aguilar, S. Y. Herasimenka, J. Karas, H. Jain, J. Lee, K. Munoz, L. Michaelson, T. Tyson, W. J. Dauksher, and S. Bowden, *Proc. 2016 IEEE 43rd Photovolt. Spec. Conf*, 1972 (2016).
8. J. Geissbuhler, S. de Wolf, A. Faes, N. Badel, Q. Jeangros, A. Tomasi, L. Barraud, A. Descoeudres, M. Despeisse, and C. Ballif, IEEE J. Photovoltaics 4, 1055 (2014).
9. M. Zwegers, J. Bertens and G. van de Ven, going to be published in Energy Procedia, (2017).
10. A. Lachowicz, J. Geissbühler, A. Faes, J. Champliaud, J. Hermans, J. Lerat, P. Ribeyron, C. Roux, G. Wahli, P. Papet, B. Strahm, J. Horzel, C. Ballif and M. Despeisse, going to be published in Energy Procedia, (2017).
11. M. A. Green, Prog. Photovolt: Res. Appl. 19, 911 (2011).
12. M. Hörteis, J. Benick, J. Nekarda, A. Richter, R. Preu, S. W. Glunz, E. Urrejola, K. Peter, J. Glatz-Reichenbach, E. Wefringhaus, H. Plagwitz, G. Schubert, F. S. Grasso, L. Gautero, J. Rentsch, R. Lanzafame, A. Ebong, I. B. Cooper, B. Rounsaville, K. Tate, A. Upadhyaya, A. Rohatgi, M. Hermle, J. Bartsch, A. Mondon, C. Schetter, C.

Boulord, A. Kaminski, Y. Veschetti, D. Blanc-Pelissier, B. Grange, A. Bettinelli, D. Heslinga, M. Lemiti, B.-J. Godejohann, F. Heinemeyer, C. Mader, D. Münster, T. Dullweber, N.-P. Harder, R. Brendel, D. Reinwand, P. Hartmann, P. Grunow, J. Hoornsta, and G. Beaucarne, *Proceedings of the 2nd Workshop on Metallization for Crystalline Silicon Solar Cells*. *Status, trends and new directions* (2010).
13. R. Rohit, A. Rodofili, G. Cimiotti, J. Bartsch, and M. Glatthaar, Energy Procedia 124, 901 (2017).
14. M. Glatthaar, R. Rohit, A. Rodofili, Y. Snow, J. Nekarda, and J. Bartsch, IEEE J. Photovoltaics **7**, 1569 (2017).
15. Smits, The bell system technical journal (1958).
16. S. B. Walker and J. A. Lewis, Journal of the American Chemical Society 134, 1419 (2012).
17. Reeves, IEEE Electron device letters EDL-3 (1982).
18. I. Serebrennikova and H. S. White, Electrochem. Solid-State Lett. 4, B4 (2001).
19. M. Pourbaix, *Atlas of Electrochemical Equilibria in Aqueous Solutions* (N. Ass. of Corrosion Engineers, 1974).
20. M. Rauer, A. Mondon, C. Schmiga, J. Bartsch, M. Glatthaar, and S. W. Glunz, Energy Procedia 38, 449 (2013).